JET PROPULSION LABORATORY
CALIFORNIA INSTITUTE OF TECHNOLOGY

INTEROFFICE MEMORANDUM
IOM 335-JW,DB,WF-20080314-001
July 19, 2013

To: Lunar Ephemeris Users

From: J. G. Williams, D. H. Boggs and W. M. Folkner

Subject: DE430 Lunar Orbit, Physical Librations, and Surface Coordinates

1. Introduction

The planetary and lunar ephemeris DE430 described in this memo and a companion memo (Folkner et al., 2013) is provided for missions to the Moon, Mars and other solar system bodies. This memo discusses the DE430 lunar orbit, orientation angles and surface coordinates while the companion memo discusses the planetary ephemerides. Along with the planetary orbits, the orbit and physical librations of the Moon are updated. The DE430 lunar orbit is compared with DE421, our former recommendation for the Moon. The construction of the lunar part of DE430 is described. Tables for geophysical parameters of Earth and Moon are presented. For coordinate frames rotating with the Moon, the principal axis and mean Earth/mean rotation axis frames are described and the rotation between the two frames is given. Accurate coordinates are tabulated for the five lunar retroreflector arrays including Lunokhod 1.

The DE430 lunar and planetary ephemeris has several advantages. To generate this ephemeris, up-to-date high quality data were fit for the Moon and planets. Improvements in models and model parameters include: (1) many individual asteroids perturbing the planets and Moon, (2) more accurate gravity fields for the Earth and Moon, (3) an upgraded terrestrial tidal model, and (4) improved knowledge of lunar solid-body tides.

2. DE430 vs. DE421 Orbit

The DE421 ephemeris was generated in 2008 (Folkner et al., 2008; Williams et al., 2008). Compared to DE421, five more years of lunar and planetary data were fit for DE430. This memo concentrates on the lunar aspects of DE430.

The DE430–DE421 lunar position differences are illustrated in Figure 1. The figure shows the differences in right ascension, declination, and radius from 1970 to 2020. The right ascension and declination differences reach up to ~1 m perpendicular to the radius, or up to ~1/2 milliarcsecond (mas) in angle. The prominent 18.6 yr modulation is the period of retrograde circulation of the orbit's node along the ecliptic plane. The inclination of the lunar orbit plane to the Earth's equator plane varies between 18.3˚ and 28.6˚. The prograde argument of perigee circulation takes 6 yr. For the radial difference between DE430 and DE421, the ~1/4 m shift is due to a decrease in *GM*, the gravitational constant times the mass of the Earth-Moon system. The monthly oscillation in radius growing from ~2001 is due to small differences in mean anomaly rate and acceleration, and also in eccentricity rate. The monthly radial variation is a few centimeters over the 1970-2012 span of lunar laser ranging data. DE430 agrees well with DE421.

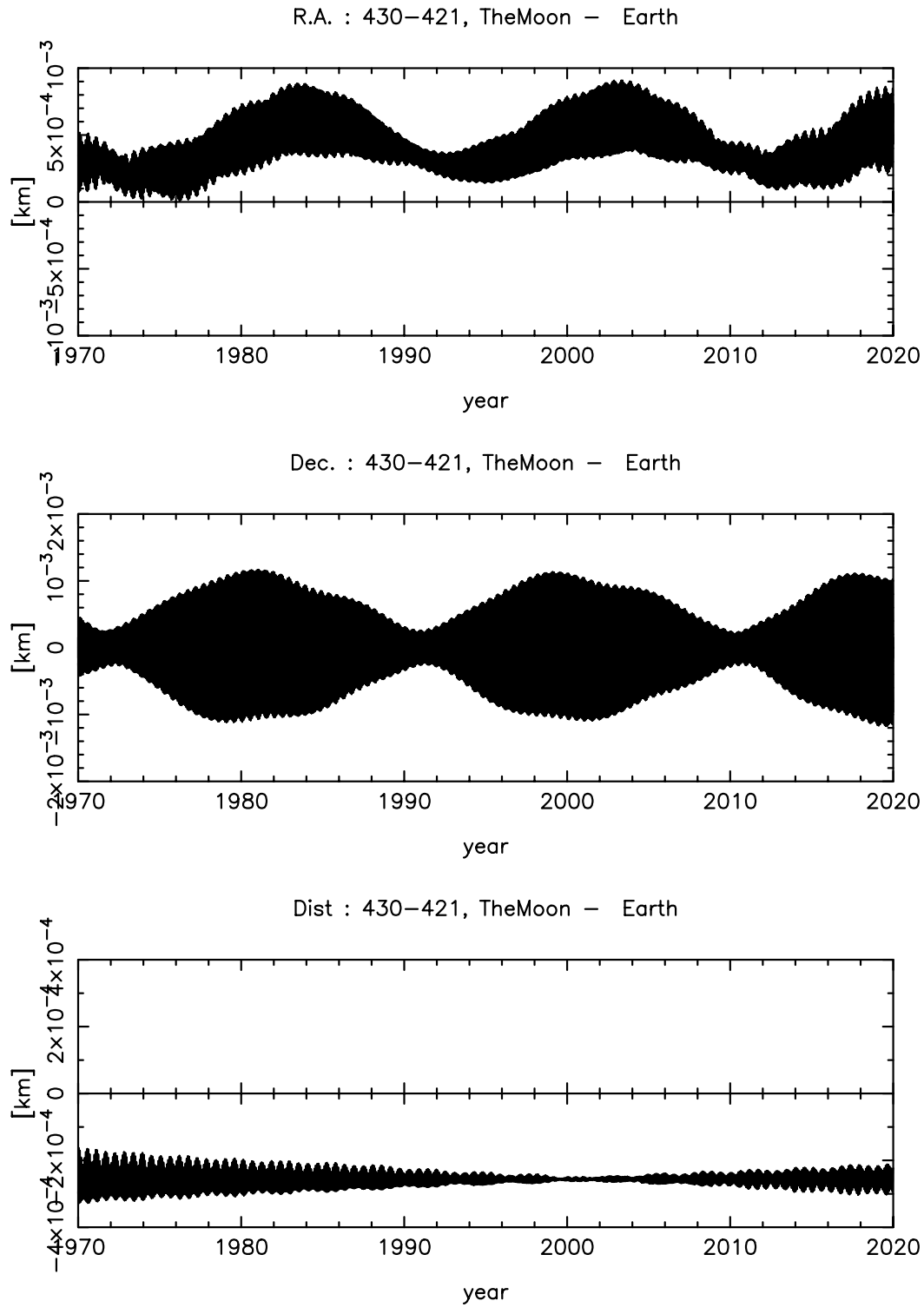

Figure 1. Lunar DE430 – DE421 differences for right ascension, declination, and radius.

3. Lunar Laser Ranges

Lunar laser ranges are the only data type analyzed to generate the DE430 lunar ephemeris and physical librations. Each Lunar Laser Ranging (LLR) measurement is the time of flight of a laser pulse fired from an observatory on the Earth to a retroreflector on the Moon, and bounced back to the observatory. It is convenient to call these time-of-flight observations ranges. For rms residuals we use the one-way range, with 15 cm/nanosec.

The DE430 lunar and planetary ephemeris results from a simultaneous fit to LLR and planetary data. The planetary data are discussed by Folkner et al. (2013). Here we address the lunar ephemeris and the physical librations, the 3-dimenional orientation of the Moon. The initial conditions at JD 2440400.5 for the lunar ephemeris and three-dimensional lunar orientation (Euler angles and spin rates) were fit along with lunar laser retroreflector array positions and other lunar parameters. The Lunar Laser Ranging (LLR) data set consisted of 18,548 ranges extending from March 16, 1970 to December 18, 2012. Modern range residuals are more than an order-of-magnitude smaller (weighted rms 1.9 cm for the past 4 yr) than residuals of the early data. Ranges were processed from three sites at McDonald Observatory, Texas, the 2.7 m telescope and two MLRS sites. Ranges from single sites at Observatoire de la Côte d'Azur, France; Haleakala Observatory, Hawaii; Apache Point Observatory, New Mexico; and Matera, Italy were also processed. See Table 1 for the number of observations analyzed from each site.

Table 1. Observations from LLR stations 1970-2012.

Site	Number of ranges	Time span
McDonald 2.7 m, Texas	3451	1970 – 1985
MLRS 1	275	1985 – 1988
MLRS 2	2919	1988 – 2012
Observatoire de la Côte d'Azur, France	9635	1984 – 2012
Haleakala, Hawaii	694	1984 – 1990
Apache Point, New Mexico	1557	2006 – 2012
Matera, Italy	17	2009 – 2010

Ranges to five retroreflector arrays on the Moon were analyzed. They are located at the Apollo 11, 14, and 15, and the Lunokhod 1 and 2 sites. A majority of the ranges are to the largest array at the Apollo 15 site (75.6%), while Lunokhod 1, recovered in 2010 (Murphy et al., 2011), has the fewest number of ranges (0.6%). Apollo 11 and 14 make up 10.5% and 10.3% of the total data set, respectively, and Lunokhod 2 has 3.0%. It appears that the return signals from the arrays have faded (Murphy et al., 2010) and Lunokhod 2 has become particularly difficult to range. Ranges to multiple arrays are important for determining the physical librations and lunar geophysical parameters. Table 2 lists the number of ranges to each lunar retroreflector array.

Table 2. Ranges to lunar retroreflectors.

Lunar Site	Number	Percentage
Apollo 11	1953	10.5%
Apollo 14	1918	10.3%
Apollo 15	14022	75.6%
Lunokhod 1	105	0.6%
Lunokhod 2	550	3.0%

4. Construction of the Ephemeris

The construction of a new ephemeris involves a series of choices and sometimes compromises. The models for the computation of both the acceleration of the Moon in its orbit and the torques about its center of mass in the numerical integration program, and the model for the computation of range for the range data fits, depend on geophysical processes in the Earth and Moon. Some of the geophysical parameters are input and held constant while others are fit to the lunar and planetary tracking data. Linear constraints between parameters can be applied. Several iterations of solutions and integrations were made.

The DE430 lunar and planetary ephemeris benefits from more high-quality data available for the Moon and planets. In addition to the LLR observations for the Moon, there are high quality ranges to Mercury, Venus, Mars, and Saturn (Folkner et al., 2013). The new integration has 323 individual asteroids perturbing the planets and Moon. Asteroid masses are no longer adjusted in blocks by taxonomic class. Both the Earth and Moon have more accurate gravity fields, and there is an improved terrestrial tidal model. More information on the improvements is given in the following sections.

4.1 System Parameters

Tables 3-5 give some parameters of interest. "Type" indicates whether a parameter was "fixed" or "free" to change during the solution leading to the DE430 integration. Some entries were "derived" from other parameters after the solution. Uncertainties for fit parameters are intended to be realistic, but are based on the solution and do not include a contribution from parameters held fixed. Quantities derived from fit parameters will have uncertainties, whereas those derived from fixed parameters do not. A few parameters are "defined" by the IAU and/or other international bodies. Values of the basic integration and fit parameters with more digits, but not the uncertainties or derived quantities, can be found among the DE430 files.

Parameters appropriate for the Earth-Moon-Sun system are given in Table 3. The first three apply to the whole solar system. We use TDB as our solar system barycentric coordinate time. There are 86400 sec in a day. See Chapter 3 of the 2010 IERS Conventions (Petit and Luzum, 2010) for a further discussion of time scales. The Sun's mass is 1 solar mass. The mass was held constant for this ephemeris, but data accuracies are approaching the expected rate of $-9\text{x}10^{-14}$ solar masses/yr (Noerdlinger, 2008). Some of the parameters are redundant and can be computed by manipulation of the others, e. g., AU/c and converting GM_{SUN} from the square of Gauss' constant in au^3/d^2 to km^3/sec^2.

The point mass accelerations for solar system bodies follow the relativistic Einstein-Infeld-Hoffmann formulation for multiple masses (Williams et al., 1996; Standish and Williams, 2012). A solar system barycentric (SSB) frame is used. Gravity field and tide effects are added on to the point mass accelerations. The DE430 "geocentric" lunar orbit results from integrating the difference of accelerations computed for Earth and Moon in an SSB frame, a distinction important for relativistic effects. See Standish and Williams for an exposition of the acceleration and torque model of the integrator.

The joint fit of lunar and planetary data used $GM_{\text{EARTH+MOON}}$ in au^3/d^2 and Earth/Moon mass ratio as independent parameters. In Table 3 we give the GMs in km^3/sec^2, and also give the dimensionless Sun/(Earth+Moon) mass ratio. The DE430 $GM_{\text{EARTH}} = 398600.4354 \pm 0.0005$

km^3/sec^2 value agrees well with the Ries et al. (1992) result of 398600.4356±0.0004 km^3/sec^2, with the uncertainty from Ries (2007), and the Dunn et al. (1999) value of 398600.4360±0.0002 km^3/sec^2. Both satellite laser ranging values have been adjusted by –0.0059 km^3/sec^2 for the relativity correction needed to convert GM_{EARTH} in a geocentric frame to an SSB frame using TDB seconds. DE421 had 398600.4362 km^3/sec^2. The DE430 GM_{MOON} value agrees with determinations from GRAIL analysis and other sources (Konopliv et al., 2013; Lemoine et al., 2013; Williams et al., 2013b).

For an elliptical orbit with semimajor axis a and eccentricity e, the time averaged radius is given by $<r> = a(1+e^2/2)$ and the inverse average is $<1/r> = 1/a$, or $a = 1/<1/r>$. The $<1/r>$ average has been evaluated using the analytical lunar ephemeris series of Chapront-Touzé and Chapront (1988, 1991), which is also the source for $<r>$. Both a and $<r>$ have been adjusted for a more recent value of $GM_{EARTH+MOON}$. The two values given in Table 3 may not be accurate to the number of digits given. Note that the average of the osculating semimajor axis $<a(t)>$ given in Chapront-Touzé and Chapront (1991) is different from the $a = 1/<1/r>$ given here. The lunar mean motion is denoted by n. We defer discussion of the three dissipation parameters dn/dt, da/dt, and de/dt until Section 4.4.

Table 3. Earth-Moon-Sun system parameters.

Parameter	Type	Unit	Value
Gauss' constant	fixed	$au^{1.5}/d$	0.01720209895
AU length	defined	km	149597870.700
Speed of light c	defined	m/sec	299792458
AU/c	fixed	sec	499.004783836
R_{SUN}	fixed	km	696000
$J_{2\ SUN}$	fit	1	$(2.1\pm0.7)10^{-7}$
Sun/(Earth+Moon)	fit	1	328900.5598±0.0004
Earth/Moon mass ratio	fit	1	81.3005691±0.0000024
GM_{SUN}	fixed	km^3/sec^2	132712440041.94
$GM_{EARTH+MOON}$	fit	km^3/sec^2	403503.2355±0.0005
GM_{EARTH}	derived	km^3/sec^2	398600.4354±0.0005
GM_{MOON}	derived	km^3/sec^2	4902.80007±0.00014
a	derived	km	384399.014
$<r>$	derived	km	385000.525
Dissipation dn/dt	derived	$"/cent^2$	–25.82±0.03
Dissipation da/dt	derived	mm/yr	38.08±0.04
Dissipation de/dt	derived	1/yr	$(1.36\pm0.04)x10^{-11}$

4.2 Parameters for the Earth

For the Earth's gravity field, zonal coefficients J_2, J_3, J_4, and J_5 were taken from the Table 6.2 low-degree gravity field in the 2010 IERS Conventions (Petit and Luzum, 2010). The equatorial Earth radius used with gravity was set to 6378.1363 km. The input J_2 coefficient is a "tide free" value, but the J_2 value was adjusted to be compatible with Love number $k_{20} = 0.335$. The constant parts of both the solid-body and ocean zonal tides are part of the k_{20} value and tidal acceleration computation here, but not in the Conventions J_2 value, where ocean tides are handled separately. An unnormalized J_2 rate of $–2.6x10^{-11}$ /yr is used with a J2000 reference time for J_2. A J_5 value and J_2 rate are added parameters new to this ephemeris.

The Earth tide gravity model for DE430 uses three Love numbers k_{20}, k_{21}, and k_{22} with five tidal time delays: one for long period tides (zonal 20), two for diurnal tides (21), and two for semidiurnal tides (22), respectively. The three Love numbers and the zonal (long period) time delay are combinations of both Earth and ocean tides. The Earth tides come from the IERS Conventions (Petit and Luzum, 2010) and the ocean tides are based on the FES2004 result (Lyard et al., 2006; reformatted by Richard Ray on a web site, 2007). Tidal response changes with frequency and the five time delays were intended to approximately match the Mf, O1, Q1, M2 and N2 tides, which are the most important tides in each of the three frequency bands for the tidal secular acceleration, semimajor axis rate, and eccentricity rate of the Moon. The K1 and solar tides are also part of the tide model, but they are not effective at perturbing the lunar orbit. DE421 used only three time delays (Williams et al., 2008), which resulted in a low eccentricity rate; see Standish and Williams (2012) for the old formulation. The new formulation for the diurnal and semidiurnal tides has separate time delays for orbit and rotation. This causes the time delay to change with tidal frequency for the two bands. The zonal time delay (Δt_{20}) value was based on the Mf ocean tide, whereas the input values of the diurnal and semidiurnal orbit delays, Δt_{21O} and Δt_{22O}, respectively, were based on the combined tide model. In contrast to those three fixed values, the diurnal (Δt_{21R}) and semidiurnal (Δt_{22R}) rotation time delays were solution parameters.

Earth-related parameters, including Love numbers and time delays, are summarized in Table 4. Tidal secular acceleration in orbital longitude, and semimajor axis rate and eccentricity rate were derived from the Love number and time delay values, using a theory. Applied after the solution was complete, the theory for the conversion is based on a uniformly precessing ellipse without periodic perturbations. The error from that theory might be as large as 1/2%, but the uncertainties in the table are internal errors, without the 1/2%, that indicate how well the orbit can be extrapolated into the past and future. There is a –0.908 correlation between the diurnal and semidiurnal rotation time delays, so the sums of the diurnal and semidiurnal tidal dn/dt, da/dt, and de/dt have smaller uncertainties than their separate parts.

The computation of the range depends on the coordinates of the ranging stations, which are fit. Station motion was fit when a station's data span extended for years. The small diurnal and semidiurnal UT1 coefficients were fixed and based on the IERS Conventions (Petit and Luzum, 2010). Two rotation angles at J2000, an X-axis rotation about the equinox direction and a Y-axis rotation about the direction toward 90˚ right ascension and 0˚ declination, are fit to orient the Earth's equator in space with respect to its orbit. The alignment of the inner four planets with the international celestial reference frame (ICRF) is established mainly through planetary VLBI data to Mars and Venus. The J2000 X-axis and Y-axis rotation rates with respect to space, converted to obliquity and equatorial precession rates for the table, were fit along with several nutation coefficients. The J2000 X- and Y-axis rotation angles fit for DE430 can be compared with 7.0 mas and –16.6 mas in Hilton et al. (2006). The X- and Y-axis rotation angles have some dependence on the secular and long-period variations. The Hilton et al. value of obliquity rate is –0.26 mas/yr while the precession of the equator, or luni-solar precession, is 50.384815 "/yr.

Table 4. Geophysical and orientation parameters for the Earth.

Parameter	Type	Unit	Value
Gauss' constant	fixed	$au^{1.5}/d$	0.01720209895
$GM_{EARTH+MOON}$	fit	km^3/sec^2	403503.2355±0.0005
Sun/(Earth+Moon)	derived	1	328900.5598±0.0004
Earth/Moon mass ratio	fit	1	81.3005691±0.0000024
GM_{EARTH}	derived	km^3/sec^2	398600.4354±0.0005
Equatorial radius	fixed	km	6378.1363
$J_{2\ EARTH}$	fixed	1	$1082.62545x10^{-6}$
dJ_2/dt	fixed	1/yr	$–2.6x10^{-11}$
k_{20}	fixed	1	0.335
k_{21}	fixed	1	0.320
k_{22}	fixed	1	0.320
Δt_{20}	fixed	day	0.0640
Δt_{21R}	fit	day	0.007363±0.000301
Δt_{21O}	fixed	day	–0.044
Δt_{22R}	fit	day	0.002535±0.000025
Δt_{22O}	fixed	day	–0.100
Zonal dn/dt	derived	$"/cent^2$	0.12
Diurnal dn/dt	derived	$"/cent^2$	–3.43±0.10
Semidiurnal dn/dt	derived	$"/cent^2$	–22.72±0.09
Earth dn/dt	derived	$"/cent^2$	–26.04±0.04
Zonal da/dt	derived	mm/yr	–0.18
Diurnal da/dt	derived	mm/yr	5.07±0.14
Semidiurnal da/dt	derived	mm/yr	33.52±0.14
Earth da/dt	derived	mm/yr	38.41±0.06
Zonal de/dt	derived	1/yr	$–0.031x10^{-11}$
Diurnal de/dt	derived	1/yr	$(0.216±0.006)x10^{-11}$
Semidiurnal de/dt	derived	1/yr	$(1.566±0.006)x10^{-11}$
Earth de/dt	derived	1/yr	$(1.751±0.003)x10^{-11}$
X-axis rotation angle	fit	mas	5.7±0.5
Y-axis rotation angle	fit	mas	–17.0±0.4
Obliquity rate	fit	mas/yr	–0.28±0.05
Luni-solar precession	fit	"/yr	50.38474±0.00007

4.3 Parameters for the Moon

Table 5 gives the lunar geophysical parameters. The reference radius used with the gravity field is 1738 km, close to the equatorial radius, though the mean radius is smaller (Smith et al., 2010; Neumann, 2013). The mass of the Moon depends on the Earth/Moon mass ratio and the *GM* of the Earth-Moon system. Planetary data analysis determines the mass ratio, whereas LLR data analysis gives $GM_{EARTH+MOON}$. The lunar mantle orientation (physical libration) initial conditions and retroreflector coordinates for Apollo 11, 14, and 15, and Lunokhod 1 and 2 were solution parameters. The coordinates are given in Section 6.3. Lunar Love number h_2 was fit while k_2 was set equal to a GRAIL-determined value. Displacement Love number l_2 was fixed to a model value. The ratio of the polar moment of inertia of the fluid core to the whole-Moon polar moment, C_f/C, was set to $7x10^{-4}$. Dissipation parameters were fit for lunar tides (time delay Δt_m)

and fluid-core/solid-mantle boundary (CMB) interaction (K_v/C); see Williams et al. (2001) for more detailed definitions.

Table 5. Geophysical parameters for the Moon.

Parameter	Type	Unit	Value
Earth/Moon mass ratio	fit	1	81.3005691±0.0000024
GM_{MOON}	derived	km^3/sec^2	4902.80007±0.00014
Reference radius R	fixed	km	1738.0
$(C–A)/B$	fit	1	$(631.0213±0.0031)x10^{-6}$
$(B–A)/C$	fit	1	$(227.7317±0.0042)x10^{-6}$
$J_{2\ MOON}$	fixed	1	$203.21568x10^{-6}$
$C_{22\ MOON}$	derived	1	$22.38274x10^{-6}$
C/MR^2	derived	1	0.393142
I/MR^2	derived	1	0.393007
k_2	fixed	1	0.024059
h_2	fit	1	0.0476±0.0064
l_2	fixed to model	1	0.0107
Δt_m	fit	day	0.0958±0.0109
K_v/C	fit	1/day	$(1.6366±0.135)x10^{-8}$
Tidal dn/dt	derived	$"/cent^2$	0.199±0.023
CMB dn/dt	derived	$"/cent^2$	0.018±0.002
Moon dn/dt	derived	$"/cent^2$	0.217±0.021
Tidal da/dt	derived	mm/yr	–0.294±0.033
CMB da/dt	derived	mm/yr	–0.027±0.002
Moon da/dt	derived	mm/yr	–0.321±0.031
Tidal & Moon de/dt	derived	1/yr	$(–3.92±0.45)x10^{-12}$
Fluid moment ratio C_f/C	fixed	1	$7x10^{-4}$
CMB flattening f	fit	1	$(2.46±0.28)x10^{-4}$
$[C_f–(A_f+B_f)/2]/C$	derived	1	$(1.73±0.20)x10^{-7}$

A definite advantage for DE430 is the much improved k_2 and gravity field values resulting from GRAIL data analysis (Konopliv et al., 2013; Lemoine et al., 2013). A GRAIL solution prior to the final GL0660B solution of Konopliv et al. provided DE430 with k_2 and gravity field values through degree and order 6. Exceptions were made for three degree-3 coefficients, C_{32}, S_{32}, and C_{33}, that were chosen as solution parameters to provide a better fit to the LLR data. These small differences from the GRAIL values probably indicate unmodeled effects in the physical libration model. C_{22} is calculated from J_2 and the two lunar moment of inertia differences $\beta = (C–A)/B$ and $\gamma = (B–A)/C$, where $A<B<C$ are the three principal moments of inertia. The tabulated parameters J_2, C_{22}, $(C–A)/B$, and $(B–A)/C$ do not include the permanent tide contributions. They are analogous to "tide free" Earth zonal coefficients. The values for the normalized polar moment C/MR^2 and mean moment I/MR^2 do include the effect of the permanent tide.

In Table 5, both K_v/C and f demonstrate the existence of a fluid core. The fluid core moment-of-inertia ratio C_f/C is fixed. The CMB flattening f is very sensitive to the choice of the moment ratio C_f/C value. Assuming a uniform fluid core, the product $f\,C_f/C = [C_f–(A_f+B_f)/2]/C$ is less sensitive to the choice of C_f/C than is f. The uncertainty tabulated for f is internal and does not include a plausible spread for the C_f/C ratio. However, with the moment ratio spread in the

Appendix of Williams et al. (2013b), that paper obtains $(2.46\pm1.4)\times10^{-4}$ for flattening f and $(1.73\pm0.5)\times10^{-7}$ for $[C_f-(A_f+B_f)/2]/C$.

A compromise is made for the dependence of the Moon's tidal dissipation on frequency. The integration uses a single time delay model for the Moon, corresponding to a tidal Q proportional to 1/frequency, but fits with parameters sensitive to the frequency dependence support only a weak dependence on frequency (Williams et al., 2001; Williams et al., 2013b). The different tidal frequency dependences cause physical libration effects at the few milliseconds of arc (mas) level, which are not present in the integration; these are detectable with the LLR fits, but are not troublesome to most users. The three additional periodic terms for longitude libration τ are given by eq. (1) and their sum is plotted in Figure 2. The rms deviation is 4.5 mas and the peak correction is 10 mas. An arc of 1 mas is 8.4 mm on the surface.

$$\Delta\tau = (5.0\pm1.3)\cos l' + (1.5\pm1.2)\cos(2l-2D) - (3.6\pm3.3)\cos(2F-2l) \quad \text{mas} \qquad (1)$$

Orbit-related Delaunay arguments are l for lunar mean anomaly (27.555 d period), l' for solar (or Earth-Moon center of mass) mean anomaly (365 d), F for argument of latitude (27.212 d), and D for elongation of Moon from Sun (29.531 d). These angles are represented by polynomials in time and do not include periodic perturbations; see eqs. (5.43) in Petit and Luzum (2010).

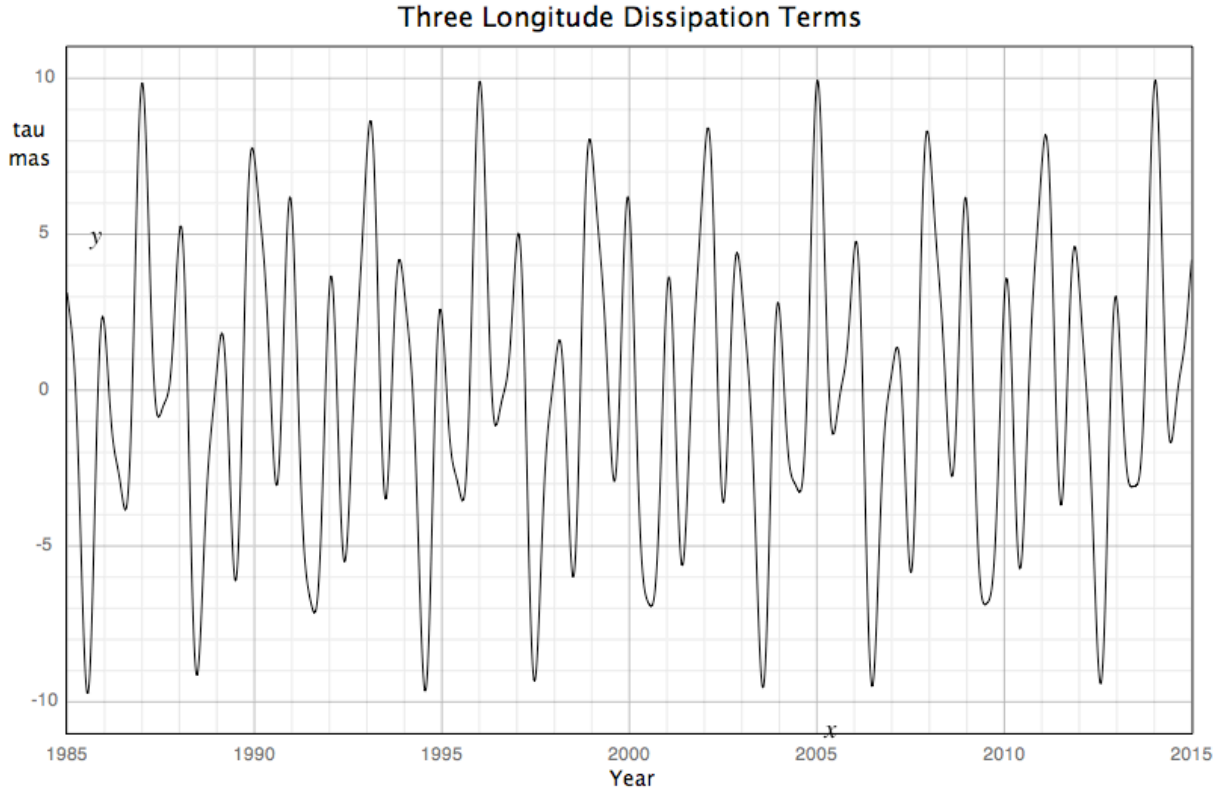

Figure 2. Sum of three additional dissipation terms in longitude librations (τ).

The integrator's initial (MJD 40400) conditions for both the mantle and core rotation are specified by three Euler angles and three spin rate components. The differential equations for the fluid core rotation only involve the core's angular spin rate vector. Still, core Euler angles are

integrated and steady state theory is used for the initial core Euler angles. Flattening f of the CMB and the initial angular rate vector for the fluid core orientation are fit. The fluid core Euler angles were constrained during early LLR-only iterations with the following approximate expressions.

$$\begin{aligned} \phi_c &= 7.21\ \text{x}10^{-5} - 1.1359\text{x}10^{5}\ K_v/C - 2.573\ f \\ \theta_c &= 0.4095211 - 2.183\text{x}10^{4}\ K_v/C + 7.537\ f \\ \psi_c &= -0.352768 - 2.32324\text{x}10^{7}\ K_v/C + 1095.9\ f \end{aligned} \qquad (2)$$

Those three core Euler angles were held fixed at $-2.4199\text{x}10^{-3}$, 0.4110195, and –0.4630947 during the final joint lunar and planetary iterations.

4.4 Tidal Acceleration

When the dissipation effects from Earth and Moon are added together, the resulting acceleration in orbital mean longitude is –25.82±0.03 "/cent^2, the semimajor axis rate is 38.08±0.04 mm/yr, and the eccentricity rate is $(1.36\pm0.04)\text{x}10^{-11}$ (Table 3). The inclination rate di/dt is not tabulated; it is only –0.9 μas/yr. These derived values depend on a theory that is not accurate to the number of digits given. The uncertainty in the conversion for Earth tides could be as much as ~1/2% of the total. The uncertainties in Tables 3-5 are internal accuracies that indicate how well the orbit can be projected into the past and future. For example, the ±0.03 "/cent^2 uncertainty in mean longitude acceleration grows to ±0.15 mas (±28 cm) in longitude after a decade, about ±1.5 cm in radius. With a 1/2% uncertainty, the dn/dt uncertainty is ±0.13 "/cent^2 and the da/dt uncertainty is ±0.19 mm/yr.

For an elliptical orbit, the time-averaged mean distance is $a(1+e^2/2)$. For the Moon a = 384,399 km and the mean distance is 385,000 km including solar perturbations. For DE430, the rate of tidal increase of the mean distance is 38.43 mm/yr, slightly larger than the semimajor axis rate. The tide-induced rates for perigee and apogee distances are 30.8 and 45.4 mm/yr, respectively. It should be appreciated that the gravitational interaction of the Moon with the Sun and planets is strong and the perturbations are large. The solar perturbations amount to thousands of kilometers. Apart from the tidal and CMB dissipation effects, these gravitational forces are conservative. LLR data analysis distinguishes the perturbations due to the weak dissipative forces from the perturbations due to the conservative forces, but this cannot be done from casual inspection of either the LLR data or the integrated lunar ephemeris.

Comparisons between different ephemerides are instructive; e.g., the computed DE430–DE421 tidal acceleration difference is only 0.03 "/cent^2, which is too small to be obvious in the right ascension and declination plots of Figure 1, although it contributes to the buildup of the monthly oscillation in radius difference. Tidal dissipation in Earth and Moon also causes an eccentricity rate. Past solutions revealed an anomalous eccentricity rate when using DE421 (Williams and Boggs, 2009) and earlier ephemerides (Williams et al., 2001). The terrestrial tidal dissipation model with five time delays that was used to integrate DE430 has reduced the anomalous rate by more than 50%, so at least part of that "anomalous" rate was coming from tides, as predicted in the 2009 paper. LLR fits after generating DE430 find an extra eccentricity rate of $(5\pm2)\text{x}10^{-12}$ /yr, or –2 mm/yr in perigee distance and +2 mm/yr in apogee distance (Williams et al., 2013a). Only two of the five time delays were solution parameters when DE430 was created; we could have adjusted the other time delays to increase the tidal eccentricity rate and reduce the "anomalous" rate, but we decided to stay close to the FES2004 tide model (Lyard et al., 2006;

Ray, 2007). The LLR model for tides is compact compared to the model used for artificial satellites (Chapter 6 of Petit and Luzum, 2010), and it may need further improvement to match eccentricity rate.

5. Lunar Coordinate Frames — Principal Axes and Mean Earth/Mean Rotation Axes

The lunar physical librations can be described by three Euler angles that rotate from space to body-fixed axes. The equations of motion for lunar Euler angles based on a principal axis (PA) system are known (Eckhardt, 1981; Williams et al., 2001; Standish and Williams, 2012). The center of mass is the origin of this Moon-fixed system. The vector differential equations of motion are integrated numerically. The principal axes of the lunar moment-of-inertia matrix are used for the X, Y and Z coordinate directions. These are principal axes of the matrix before tidal distortions are applied. The LLR solutions give six initial conditions for lunar orientation Euler angles along with lunar laser retroreflector array coordinates.

Another Moon-centered system of interest has the mean direction toward the Earth for the X axis and the mean direction of rotation for the Z axis. Y completes the right-handed triad. This system is an idealization; a practical attempt to determine these mean directions with high accuracy would depend on the approach and time interval used. In Lunar Laser Ranging (LLR) papers we have called this system the mean Earth/mean rotation axis system or, more tersely, the mean Earth/rotation axis (MER) system. In the Archinal et al. (2011ab) IAU/IAG working group exposition on coordinates and rotations, this system is referred to as the mean Earth/rotation axis system or the mean Earth/polar axis system. Davies et al. (2000) and earlier IAU/IAG working group papers (Seidelmann et al., 2007, and earlier papers in this sequence) use the latter name. These three names refer to the same system.

An ellipsoidal Moon with only a second-degree (gravity) figure would have coinciding mean axis and principal axis systems. Third- and higher-degree coefficients of the gravity field affect the Euler angles, and cause a constant 3-axis rotation between the PA and MER frames. There is also a small constant rotation due to dissipation effects in the Moon. Knowledge of the gravity field and dissipation has improved strongly with time. Konopliv et al. (2013) and Lemoine et al. (2013) present high-accuracy gravity fields derived from data gathered by NASA's GRAIL mission. This memo and Williams et al. (2013b) give compatible LLR results.

A constant three-angle rotation relates the PA and MER frames, but our knowledge of the three constant angles depends on the gravity field coefficients, and a physical libration theory or representation is required to establish the three angles. Since gravity field coefficients can change for different ephemerides, the rotation angles must be compatible with the ephemeris. The gravity harmonic coefficients have improved over the years (Konopliv et al., 1998, 2001, 2013). A product of the GRAIL mission, the GL0660B gravity field (Konopliv et al., 2013) is recommended for spacecraft orbit calculations using DE430. Subsequent fields determined from GRAIL data analysis should be compatible. For DE430 the Love number k_2 plus degree and order 2-6 gravity field coefficients were adopted from a precursor solution to GL0660B that is nearly the same. However, three third-degree coefficients C_{32}, S_{32}, and C_{33} were fit to the LLR data. The moment of inertia differences $\gamma = (B–A)/C$ and $\beta = (C–A)/B$ that adjust the relation between C_{22} and J_2 were also fit during the LLR data analysis. Prior to the application of tidal distortions, C_{21}, S_{21} and S_{22} are zero, consistent with principal axis coordinates.

The LLR fits to lunar rotation and orbit are done simultaneously, and the numerical integration for orbit and Euler angle evolution is simultaneous. Thus, the lunar Euler angles (physical librations) and orbit of the DE ephemeris are compatible, and the Euler angles refer to a principal axis frame. The formerly recommended ephemeris DE421 is compatible with the LP150Q gravity field (Konopliv, 2001).

6. Moon-Centered Coordinates

6.1 Deriving 3-Axis Rotations

We do not have simple equations of motions for Euler angles referred to mean Earth/mean rotation axes. Rotating from space to principal axes, the numerically integrated Euler angles that are provided with the ephemeris files are generated with high accuracy. For a given gravity field, the constant three-angle rotation from principal axes to mean axes is less accurately known than the integrated Euler angles. The fits to the LLR data use the lunar orbit and physical libration Euler angles from the numerical integration, so the resulting retroreflector array coordinates are based on the principal axis frame. The constant 3-axis rotation is typically derived after the LLR fit and integration.

How is the 3-axis rotation derived? We need a representation of physical librations that has explicit constant rotation angles. The options include a theoretical series, and a Fourier fit to a numerical integration.

At first, LLR used a sequence of theories by Eckhardt, most recently Eckhardt (1981), to establish the constant parts of the libration parameters p_1, p_2, and τ. The first two of these parameters are Moon-fixed x and y components of the unit vector normal to the ecliptic plane, and the τ parameter refers to the longitude rotation. The constant parts p_{1c}, p_{2c}, and τ_c depend mainly on the gravity field and slightly on dissipation effects. Knowledge of the gravity field was poor in earlier times and consequently Eckhardt's (1981) constant part of the τ angle is a factor of about three times larger than the modern more accurate value of the angle! Although Eckhardt provided partial derivatives with respect to the third-degree gravity coefficients, higher-degree coefficients and nonlinearities in the differential corrections limit the accuracy at some level. The last set of LLR array coordinates that directly used Eckhardt's (1981) theory for the 3-axis rotation was given in Williams, Newhall and Dickey (1987).

Note that the semianalytical series expressions for lunar angle W along with pole right ascension and declination that are given in the IAU/IAG working group documents (Archinal et al., 2011a, and earlier reports) are approximations of much lower accuracy than the numerical integrations. By comparing with integrated values, Konopliv et al. (2001) demonstrated that the series expressions for orientation lead to position errors that can exceed 100 m. One of us (JGW) derived the lunar series expressions and that uncertainty is consistent with the level of truncation of the series.

After theoretical values of p_{1c}, p_{2c}, and τ_c have been used to rotate Moon-centered retroreflector coordinates from principal axis to mean Earth/mean rotation axis coordinates, it is possible to fit the three rotation angles between a newer set of PA coordinates and an older set of MER coordinates. Then the new set of three angles is used to rotate the new PA set of coordinates into a new MER set. This procedure produces consistency among the different MER sets of coordinates, but as the accuracy of the PA coordinates improves with improving data quality and

modeling, the accuracy of the alignment of the MER frame with the real directions toward the mean Earth and mean rotation axis does not improve.

The numerically integrated Euler angles are not theories, but Fourier analysis can convert the Euler angles into a series of periodic terms resembling theories. DE403 was Fourier analyzed by Newhall and Williams (1997), and DE421 was analyzed by Rambaux and Williams (2011). Both efforts produced the p_{1c}, p_{2c}, and τ_c libration parameters as well as polynomial functions of time and periodic terms. The τ series has many long-period terms and these are a concern. Terms with periods comparable to or longer than the sampled time span will affect the polynomial terms and can bias τ_c. One of the fluid core modes damps exponentially, so backward integrations have a growing error that forward integrations do not have; consequently, Rambaux and Williams analyzed a 1070 yr integration starting in 1969. With a J2000 reference time for the polynomial terms, any misfit may corrupt the τ determination at the ends of the span more than the middle section. The largest long-period term is caused by Venus perturbations with a 273 yr period and a 14.6" amplitude. The amplitude and phase of this term change significantly over the 1070 yr span. Linear Poisson terms were fit for this variation, but any nonlinearity in the change could corrupt the fit for τ_c.

A theory and program were developed in order to overcome the less accurate gravity field that Eckhardt (1981) used. The theory balances the C_{22} torque from the τ_c rotated X and Y principal axes against the torques from the third- and fourth-degree coefficients. A small contribution from tide and core dissipation (Williams et al, 2001) is also added. Parameters p_{1c} and p_{2c} are not calculated by the program. This torque balance approach was used to compute the τ_c for the DE421 coordinate rotations (Williams, Boggs, and Folkner, 2008). Here, the DE430 orientation from PA to MER axes used a fit to the DE421 parameters p_{1c}, p_{2c}, and τ_c by Rambaux and Williams (2011), with modification for the small difference between the DE430 and DE421 PA coordinates.

6.2 The 3-Axis Rotation for DE430

If M is a vector from the center of mass to a surface point in the mean Earth/mean rotation (MER) axis frame and P is the vector in the principal axis (PA) frame, then the rotation from the PA frame to the MER frame follows the form

$$M = R_x(-p_{2c})\, R_y(p_{1c})\, R_z(-\tau_c + I^2\sigma_c/2)\, P \quad , \tag{3}$$

where p_{1c}, p_{2c}, and τ_c are the constant parts of the three libration parameters. The mean tilt of the lunar equator plane to the ecliptic plane is $I = 0.02692$ radians, and σ_c is the constant offset of the intersection of the equator plane with the ecliptic plane from the descending node of the orbit plane. Although p_1 and p_2 are coordinates, they are small and are conventionally expressed as angles. The three rotation angles are small and eq. (3) is only first order in the rotations. If the order of the Y and Z rotations is reversed, the second-order difference $R_z R_y - R_y R_z$ is a rotation about the X-axis by –0.026", 0.22 m for a point on the great circle along longitudes ±90°. The error in the first-order expression is estimated to be half that, 0.013" or ≤0.11 m in position. For DE430, the 3-axis rotation between frames is

$$M = R_x(-0.285")\, R_y(-78.580")\, R_z(-67.573")\, P \, , \tag{4}$$

where the angles are in seconds of arc and the right-handed rotations are around the body X, Y, and Z axes. The inverse rotation is

$$P = R_z(67.573") R_y(78.580") R_x(0.285") M \quad . \tag{5}$$

Note that the rotation of coordinates of eqs. (3)-(5) above and the corresponding rotation of the frames have the opposite sense. The PA X axis is 67.570" (~569 m) east and 78.580" (~662 m) south of the MER X axis. The PA Y axis is 67.570" (~569 m) east and 0.285" (~2 m) north of the MER Y axis. The PA Z axis is tilted 78.580" (~662 m) toward longitude zero and 0.285" (~2 m) toward 90˚ west. On the lunar surface with mean radius 1737.151 m (Neumann, 2013), an arc of 1" corresponds to 8.42 m.

At J2000 Rambaux and Williams (2011) found $p_{1c} = -78.513"$, $p_{2c} = 0.290"$, $\tau_c = 67.753"$, and $I\sigma_c = -0.249"$ for DE421. The difference between the LLR PA coordinates for DE430 and DE421 gives adjustments for the three angles of –0.067", –0.005", –0.183", respectively. The angles in eqs. (4) and (5) result.

If one wishes the time-varying orientation of the lunar mean Earth/mean rotation axes with respect to space, we recommend first extracting the Euler angles orienting the principal axes from the file, and then rotating by the three constant angles of eq. (4).

6.3 Retroreflector Coordinates

The LLR retroreflector array principal axis coordinates were determined during the solution leading to DE430. These PA coordinates are given in Table 6. Equation (4) was used to rotate the LLR principal axis array coordinates of Table 6 to the mean Earth/mean rotation axis frame. These MER coordinates are given in Table 7.

Table 6. Lunar laser retroreflector array coordinates using a frame based on principal axes and center of mass.

Array	*X*	*Y*	*Z*	*R*	E Longitude	Latitude
	meters	meters	meters	meters	degrees	degrees
Apollo 11	1591966.550	690699.375	21003.866	1735472.353	23.4543587	0.6934494
Apollo 14	1652689.504	-520997.525	-109730.417	1736335.734	-17.4970524	-3.6233098
Apollo 15	1554678.231	98095.485	765005.355	1735476.972	3.6104039	26.1551968
Lunokhod 1	1114292.213	-781298.510	1076058.872	1734928.585	-35.0366497	38.3331055
Lunokhod 2	1339363.318	801871.862	756358.849	1734638.663	30.9088010	25.8510123

Table 7. Lunar laser retroreflector array coordinates using a frame based on mean Earth/mean rotation axes and center of mass.

Array	*X*	*Y*	*Z*	*R*	E Longitude	Latitude
	meters	meters	meters	meters	degrees	degrees
Apollo 11	1591748.076	691220.843	20398.420	1735472.352	23.4730244	0.6734595
Apollo 14	1652818.172	-520455.918	-110360.813	1736335.734	-17.4786937	-3.6441535
Apollo 15	1554937.340	98603.741	764413.168	1735476.972	3.6284572	26.1334178
Lunokhod 1	1114957.971	-780934.909	1075633.109	1734928.585	-35.0080312	38.3151827
Lunokhod 2	1339388.601	802309.554	755849.750	1734638.662	30.9221056	25.8323282

The torque balance program gives a Z-axis rotation of 67.731" for the DE430 gravity field. This value is 0.16" larger than the rotation from Rambaux and Williams (2011). The solution leading to DE430 solved for C_{32}, S_{32}, and C_{33} rather than adopting the corresponding GL0660B values. The C_{32} difference should cause a p_{1c} change of –0.06" and the C_{33} difference should cause a τ_c change of 0.02". We conclude that the R_z rotation is uncertain by 0.2" (1.7 m on the equator) and the R_y rotation is uncertain by <0.1", affecting the MER coordinate uncertainties. By contrast, the DE430 PA retroreflector coordinates are known to decimeters for the given gravity field, but would shift up to 0.5 m in latitude if an all-GRAIL gravity field were imposed.

The LLR range model includes solid-body tides on the Moon. That calculation includes constant displacements, much of it in the mean Earth direction, in addition to variations with time. The constant parts of the tidal displacements, different for each retroreflector array, are not included in the coordinates of Tables 6 and 7, but they are given in Table 8. These permanent tidal displacements can be added to the positions in Tables 6 and 7 if precise LLR positions are to be used without a tide model. The lunar displacement Love numbers from the solution leading to DE430 are $h_2 = 0.0476$ (fit) and $l_2 = 0.0107$ (fixed to a model value), giving few decimeter constant tidal displacements as shown. A great arc of 1˚ has a 30.3 km length, and a 1" arc is 8.42 m long.

Table 8. Constant tidal displacements from Earth and Sun using $h_2 = 0.0476$ and $l_2 = 0.0107$.

Array	ΔX	ΔY	ΔZ	ΔR	ΔEast	ΔNorth
	meters	meters	meters	meters	meters	meters
Apollo 11	0.489	0.048	0.001	0.467	-0.151	-0.004
Apollo 14	0.538	-0.046	-0.010	0.526	0.118	0.024
Apollo 15	0.459	0.006	0.044	0.431	-0.023	-0.163
Lunokhod 1	0.203	0.044	-0.061	0.073	0.152	-0.135
Lunokhod 2	0.315	-0.002	-0.002	0.242	-0.164	-0.120

In the solution leading to DE430, the X coordinate of each array correlates about +0.9 with both $GM_{EARTH+MOON}$ and the osculating semimajor axis at the epoch. The mean motion is very well determined, any $GM_{EARTH+MOON}$ change is related to change in the mean semimajor axis a through Kepler's third law. The differences $a–X$ should be better determined than either a or X separately. For DE430–DE421, the MER X coordinates shift an average of –0.36 m, the constant tidal displacements of X increase an average of +0.08 m, and the $GM_{EARTH+MOON}$ change implies a semimajor axis difference of –0.26 m (see radius in Figure 1). When constant tidal displacements are included in X, the $a–X$ differences are preserved within a few centimeters.

The $GM_{EARTH+MOON}$ uncertainty implies that the semimajor axis a has an uncertainty of ~0.2 m that contributes to the X coordinate uncertainty. There is also uncertainty in the coordinates due to the orientation of the principal axes. For the DE430 gravity field and physical librations, the retroreflector PA coordinates are uncertain by 0.12 m to 0.27 m. The five retroreflector array positions are the most accurately known positions on the Moon.

7. DE430 Files

For the highest accuracy lunar navigation or scientific purposes, we recommend using the DE430 ephemeris file with the GL0660B gravity field or a compatible GRAIL-derived lunar field.

The DE430 directory is available at

ftp://ssd.jpl.nasa.gov/pub/eph/planets/ascii/de430 .

Individual ascii files, with names of the form ascpxxxx.430, will be found there. As a result of the large number of additional perturbing asteroids, modified software is provided at

ftp://ssd.jpl.nasa.gov/pub/eph/planets/ .

The SPICE kernal version of DE430 is located at

ftp://ssd.jpl.nasa.gov/pub/eph/planets/bsp/de430.bsp .

The ascii and SPICE kernel versions cover the time span from December 21,1549 on the Julian calendar to January 25, 2650 on the Gregorian calendar, or JD 2287184.5 to JD 2688976.5. Since the initial integration epoch was June 28, 1969 (Gregorian calendar), or JD 2440400.5, both forward and backward integrations were required. For both directions, the lunar tidal acceleration error accumulates as t^2. For the Moon we caution that backward integrations are less accurate than forward integrations. The CMB dissipation, with parameter K_v/C, causes core rotation modes to damp exponentially with time. When integrating backward, those modes grow exponentially. Errors in physical librations cause errors in the orbit because of coupling through the lunar gravity field. From a comparison of different integrations, it appears that the error in the DE430 orbit at 1800 is ~0.1" and the error at 1600 is ~1".

We have generated an alternative ephemeris named DE431 with a zero value for K_v/C. It does not give as good a fit to the LLR data as DE430, but it can be integrated backward for longer times. That ephemeris is suitable for analyzing ancient astronomical data. DE431 will be the subject of a separate memo.

8. Summary

The DE430 lunar positions and orientations should be improved over those of DE421 for modern times and for future years. Although DE430 is an improvement over DE421, Figure 1 shows that both are more similar to one another than to older lunar ephemerides. For high accuracy purposes, such as lunar navigation or scientific analyses, we recommend using the DE430 ephemeris with the GRAIL GL0660B gravity field or a field of comparable accuracy. Tables 1 and 2 give the distributions of lunar laser ranging (LLR) data by ranging station and retroreflector array, respectively. Table 3 presents parameters important to the Earth-Moon-Sun system. Tables 4 and 5 give geophysical parameters for the Earth and Moon, respectively. Tabulated uncertainties are internal; see the text for discussion and qualifications. Rotation of Moon-centered coordinates between the mean Earth/mean rotation axis frame (MER) and the principal axis frame (PA) can be achieved with eqs. (4) and (5). Coordinates of the lunar laser retroreflector arrays are listed in Table 6 for a PA frame and Table 7 for an MER frame. Section 7 describes the DE430 files.

Acknowledgments. We thank the JPL and GSFC data analysis groups for gravity fields determined from analyses of the GRAIL mission data. The research described in this paper was carried out at the Jet Propulsion Laboratory of the California Institute of Technology, under a contract with the National Aeronautics and Space Administration.

References

Archinal, B. A., M. F. A'Hearn, E. Bowell, A. Conrad, G. J. Consolmagno, R. Courtin, T. Fukushima, D. Hestroffer, J. L. Hilton, G. A. Krasinsky, G. Neumann, J. Oberst, P. K. Seidelmann, P. Stooke, D. J. Tholen, P. C. Thomas, and I. P. Williams (2011a), Report of the IAU working group on cartographic coordinates and rotational elements: 2009, *Celestial Mechanics and Dynamical Astronomy, 109 (2)*, 101–135, doi 10.1007/s10569-010-9320-4.

Archinal, B. A., et al. (2011b), Erratum to: Reports of the IAU Working Group on Cartographic Coordinates and Rotational Elements: 2006 & 2009, *Celes. Mech. & Dyn. Astron.*, *110* (4), 401–403, doi 10.1007/s10569-011-9362-2.

Chapront-Touzé, M., and J. Chapront (1988), ELP 2000-85: a semi-analytical lunar ephemeris adequate for historical times, *Astron. Astrophys.*, *190*, 342–352.

Chapront-Touzé, M., and J. Chapront (1991), *Lunar Tables and Programs from 4000 B. C. to A. D. 8000*, Willmann-Bell, Richmond.

Davies, M. E., and T. R. Colvin (2000), Lunar coordinates in the regions of the Apollo landers, *J. Geophys. Res., 105,* 20277–20280.

Dickey, J. O., P. L. Bender, J. E. Faller, X X Newhall, R. L. Ricklefs, J. G. Ries, P. J. Shelus, C. Veillet, A. L. Whipple, J. R. Wiant, J. G. Williams, and C. F. Yoder (1994), Lunar Laser Ranging: a Continuing Legacy of the Apollo Program, *Science*, *265*, 482–490.

Dunn, P., M. Torrence, R. Kolenkiewicz, and D. Smith (1999), Earth scale defined by modern satellite ranging observations, *Geophys. Res. Lett.*, *26* (10), 1489–1492, doi: 10.1029/1999GL900260.

Eckhardt, D. H. (1981), Theory of the libration of the Moon, *Moon and Planets, 25*, 3–49.

Folkner, W. F., J. G. Williams, D. H. Boggs (2008), Planetary ephemeris DE421 for Phoenix navigation, IOM 343R-08-002, February 13, 2008.

Folkner, W. F., D. H. Boggs, and J. G. Williams, (2013), Planetary ephemeris DE430, IOM 343R-, in preparation.

Hilton, J. L., N. Capitaine, J. Chapront, J. M. Ferrandiz, A. Fienga, T. Fukushima, J. Getino, P. Mathews, J.-L. Simon, M. Soffel, J. Vondrak, P. Wallace, and J. Williams (2006), Report of the International Astronomical Union division 1 working group on precession and the ecliptic, *Celestial Mechanics and Dynamical Astronomy*, *94*, 351–367, doi:10.1007/s10569-006-0001-2.

Konopliv, A. S., A. B. Binder, L. L. Hood, A. B. Kucinskas, W. L. Sjogren, and J. G. Williams, Improved gravity field of the Moon from Lunar Prospector, *Science, 281*, 1476–1480, 1998.

Konopliv, A. S. (2000), LP150Q file submitted to PDS website on 27 November 2000. http://pds-geosciences.wustl.edu/lunar/lp-l-rss-5-gravity-v1/lp_1001/sha/jgl150q1.lbl

Konopliv, A. S., S. W. Asmar, E. Carranza, W. L. Sjogren, and D. N. Yuan (2001), Recent gravity models as a result of the lunar prospector mission, *Icarus, 150*, 1–18.

Konopliv, A. S., R. S. Park, D.-N. Yuan, S. W. Asmar, M. M. Watkins, J. G. Williams, E. Fahnestock, G. Kruizinga, M. Paik, D. Strekalov, N. Harvey, D. E. Smith, and M. T. Zuber (2013), The JPL lunar gravity field to spherical harmonic degree 660 from the GRAIL primary mission, *J. Geophys. Res.*, online July 9, 2013, doi:10.1002/jgre.20097.

Lemoine, F. G., S. Goossens, T. J. Sabaka, J. B. Nicholas, E. Mazarico, D. D. Rowlands, B. D. Loomis, D. S. Chinn, D. S. Caprette, G. A. Neumann, M. T. Zuber, D. E. Smith (2013), High degree gravity models from GRAIL Primary mission data, *J. Geophys. Res.*, in press.

Lyard, F., F. Lefevre, T. Letellier, and O. Francis (2006), Modeling the global ocean tides: insights from FES2004, *Ocean Dynamics, 56*, 394–415.

Murphy Jr., T. W., E. G. Adelberger, J. B. R. Battat, C. D. Hoyle, R. J. McMillan, E. L. Michelsen, R. L. Samad, C. W. Stubbs, and H. E. Swanson (2010), Long-term degradation of optical devices on the Moon, *Icarus*, *208*, 31-35, doi:10.1016/j.icarus.2010.02.015.

Murphy Jr., T. W., E. G. Adelberger, J. B. R. Battat, C. D. Hoyle, N. H. Johnson, R. J. McMillan, E. L. Michelsen, C. W. Stubbs, and H. E. Swanson (2011), Laser ranging to the lost Lunokhod 1 reflector, *Icarus*, *211*, 1103-1108, doi:10.1016/j.icarus.2010.11.010.

Neumann, G. A. (2013), LRO Lunar Orbiter Laser Altimeter, PDS release of 15 March 2013, http://imbrium.mit.edu/DATA/LOLA_SHADR/.

Newhall, X X, and J. G. Williams (1997), Estimation of the Lunar Physical Librations, *Celestial Mech. and Dyn. Astron., 66*, 21-30.

Noerdlinger, P. D. (2008), Solar mass loss, the astronomical unit, and the scale of the solar system, arXiv:0801.3807 [astro-ph].

Petit, G., and B. Luzum (eds.) (2010), IERS Conventions (2010), IERS Technical Note #36, Verlag des Bundesamts für Kartographie und Geodäsie, Frankfurt am Main 2010, 179 pp. Electronic version http://www.iers.org/TN36/

Rambaux, N., and J. G. Williams (2011), The Moon's physical librations and determination of their free modes, *Celestial Mechanics and Dynamical Astronomy*, *109*, 85-100, (online version including tables Oct 26, 2010), doi:10.1007/s10569-010-9314-2.

Ray, R. (2007), Tidal spherical harmonic coefficients, http://bowie.gsfc.nasa.gov/ggfc/tides/harm_fes04.html .

Ries, J. C., R. J. Eanes, C. K. Shum, and M. M. Watkins (1992), Progress in the determination of the gravitational coefficient of the Earth, *Geophys. Res. Lett.*, *19*(6), 529-531.

Ries, J. C. (2007), Satellite laser ranging and the terrestrial reference frame; Principal sources of uncertainty in the determination of the scale, *Geophysical Research Abstracts*, *Vol. 9*, 10809, EGU General Assembly, Vienna, Austria, April 15-20, 2007.

Seidelmann, P. K., B. A. Archinal, M. F. A'Hearn, A. Conrad, G. J. Consolmagno, D. Hestroffer, J. L. Hilton, G. A. Krasinsky, G. Neumann, J. Oberst, P. Stooke, E. F. Tedesco, D. J. Tholen, P. C. Thomas, and I. P. Williams (2007), Report of the IAU/IAG working group on cartographic coordinates and rotational elements: 2006, *Celestial Mechanics and Dynamical Astronomy, 98 (3)*, 155-180.

Smith, D. E., M. T. Zuber, G. A. Neumann, F. G. Lemoine, E. Mazarico, M. H. Torrence, J. F. McGarry, D. D. Rowlands, J. W. Head III, T. H. Duxbury, O. Aharonson, P. G. Lucey, M. S. Robinson, O. S. Barnouin, J. F. Cavanaugh, X. Sun, P. Liiva, D. Mao, J. C. Smith, and A. E. Bartels (2010), Initial observations from the Lunar Orbiter Laser Altimeter (LOLA), *Geophys. Res. Lett.*, *37*, L18204, doi:10.1029/2010GL043751.

Standish, E. M., and J. G. Williams (2012), Orbital Ephemerides of the Sun, Moon, and Planets, Chapter 8 in the Explanatory Supplement to the Astronomical Almanac, Third Edition, Eds. S. Urban and P. K. Seidelmann, U. S. Naval Observatory, Washington, D. C., University Science Books, Mill Valley, CA, 305-345, http://iau-comm4.jpl.nasa.gov/XSChap8.pdf

Williams, J. G., X X Newhall, and J. O. Dickey (1987), Lunar Gravitational Harmonics and Reflector Coordinates, in the proceedings Figure and Dynamics of the Earth, Moon and Planets, astronomical institute of the Czechoslovak academy of sciences research institute of geodesy, topography and cartography, Prague, Czechoslovakia, ed. P. Holota, 643–648.

Williams, J. G., X X Newhall, and J. O. Dickey (1996), Relativity parameters determined from lunar laser ranging, *Phys. Rev. D*, *53*, 6730-6739.

Williams, J. G., D. H. Boggs, C. F. Yoder, J. T. Ratcliff, and J. O. Dickey (2001), Lunar rotational dissipation in solid body and molten core, *J. Geophys. Res., 106*, 27933-27968.

Williams, J. G., D. H. Boggs, and W. M. Folkner (2008), DE421 Lunar Orbit, Physical Librations, and Surface Coordinates, JPL IOM 335-JW,DB,WF-20080314-001, March 14, 2008.

Williams, J. G., and D. H. Boggs (2009), Lunar Core and Mantle. What Does LLR See?, in Proceedings of 16th International Workshop on Laser Ranging, SLR – the Next Generation, October 2008, Poznan, Poland, ed. Stanislaw Schillak, 101-120. http://www.astro.amu.edu.pl/ILRS_Workshop_2008/index.php

Williams, J. G., S. G. Turyshev, and D. H. Boggs (2013a), The past and present Earth-Moon system: the speed of light stays steady as tides evolve, *Planetary Science*, submitted.

Williams, J. G., A. S. Konopliv, D. H. Boggs, R. S. Park, D.-N. Yuan, F. G. Lemoine, S. J. Goossens, E. Mazarico, F. Nimmo, R. C. Weber, S. W. Asmar, H. J. Melosh, G. A. Neumann, R. J. Phillips, D. E. Smith, S. C. Solomon, M. M. Watkins, M. A. Wieczorek, J. C. Andrews-Hanna, J. W. Head, W. S. Kiefer, I. Matsuyama, P. J. McGovern, G. J. Taylor, and M. T. Zuber (2013b), Lunar interior properties from the GRAIL mission, *J. Geophys. Res.*, in preparation.